

Chapter 4

Active and Semi-active Schemes for Rail-Counterweight System

In chapter 3, we created a tuned mass damper using a part of the counterweight mass. The numerical study showed that a passive tuned mass damper is only moderately successful in reducing the seismic response. It is primarily attributed to the fact that it is difficult to find a frequency to tune the system as the system frequency changes with the position of the counterweight along the rails and also with closing and opening of the gaps when the counterweight vibrates. In this chapter, we examine the possibility of converting the TMD to an active tuned mass damper by inserting an actuator between the damper mass and the counterweight frame and actuate the damper according to some control algorithm.

We consider the three different types of active systems. In the first one, it is assumed that full state of the system is available to calculate the actuator force. However, since it may be difficult to have sensors to measure the full state directly, next we also consider the acceleration feedback scheme. In this case, the accelerations of the system are recorded at three different points, and then they are used to estimate the state to calculate the control forces. Both these methods assume that the power to operate the actuator will be available to

apply the needed force. Although the power required to operate the actuator for a counterweight is not as high as for a civil engineering structure, it is quite possible that in an earthquake occurrence scenario the power may not be available. In such cases, an active scheme that can work with an offline power source such as a battery will be much desirable. The semi-active schemes that can change the properties of the system actively without a large power source are other possible alternative that can be used with counterweights. In this study we investigate the possibility of using a magnetorheological (MR) damper as an actuator. The reason for using the MR damper is because by passing electric current through a set of coils in the damper one can create a magnetic field in the MR fluid to change its viscous resistance almost instantaneously. In the following sections, the equation of motion and control algorithms used for the three cases are described, followed by the numerical results to demonstrate their effectiveness in reducing the guide rail stress responses.

4.1 Tuned Mass Damper with an Actuator

With an additional force f_T applied by an actuator installed between the damper mass and the counterweight frame, equations (3.1) and (3.2) in chapter 3, respectively, become

$$\mu m_c \ddot{u}_T + c_T [\dot{u}_T - \dot{u} - (1 - \mu) \dot{u}_e] + k_T [u_T - u - (1 - \mu) u_e] = -\mu m_c \ddot{x}_c + f_T \quad (4.1)$$

$$\mathbf{M}_i \ddot{\mathbf{q}}_i + \mathbf{C}_i \dot{\mathbf{q}}_i + \mathbf{K}_i \mathbf{q}_i = -\mathbf{M}_i \ddot{\mathbf{x}}_i + \mathbf{D} f_T + \mathbf{f}_i \quad (4.2)$$

where \mathbf{D} is the location vector defined as

$$\mathbf{D} = \begin{Bmatrix} -1 \\ \mu - 1 \\ 1 \end{Bmatrix} \quad (4.3)$$

Equation (4.2) can be written in terms of state vector \mathbf{z} as

$$\dot{\mathbf{z}} = \mathbf{A} \mathbf{z} + \mathbf{B} f_T + \mathbf{E} \ddot{\mathbf{x}} + \mathbf{f}^* \quad (4.4)$$

where

$$\mathbf{z} = \begin{Bmatrix} \mathbf{q}_i \\ \dot{\mathbf{q}}_i \end{Bmatrix} \quad (4.5)$$

$$\mathbf{A} = \begin{bmatrix} \mathbf{0} & \mathbf{I} \\ -\mathbf{M}_i^{-1}\mathbf{K}_i & -\mathbf{M}_i^{-1}\mathbf{C}_i \end{bmatrix} ; \quad \mathbf{B} = \begin{Bmatrix} \mathbf{0} \\ \mathbf{M}_i^{-1}\mathbf{D} \end{Bmatrix} ; \quad \mathbf{E} = \begin{Bmatrix} \mathbf{0} \\ -\mathbf{I} \end{Bmatrix} ; \quad \mathbf{f}^* = \begin{Bmatrix} \mathbf{0} \\ \mathbf{M}_i^{-1}\mathbf{f}_i \end{Bmatrix} \quad (4.6)$$

In an active control schemes, the control force is determined to minimize an objective or cost function. This minimization provides the control algorithm to calculate the control force. Although the rail-counterweight system is a nonlinear system with ever changing state matrix \mathbf{A} , in this study linear control schemes using full state-feedback and acceleration-feedback are still used to calculate the control force. To verify the effectiveness of the proposed use of the linear control schemes, especially in view of the presence of the nonlinearities in the system, numerical studied are conducted.

4.2 State-feedback Approach

Assuming that all of the quantities in the state vector \mathbf{z} can be measured, the control force can be determined using LQR (Linear Quadratic Regulator) method. This is a control scheme for linear system with objective of minimizing performance index that is a quadratic function of state and control force while satisfying the equations of motion (Kwakernaak and Sivan, 1972). For the rail-counterweight system being studied, the performance index is written as

$$J = \int_0^{\infty} (\mathbf{z}^T \mathbf{Q} \mathbf{z} + r f_r^2) dt \quad (4.7)$$

where Q and r are the weight matrix and constant for the state and the control force, respectively. The minimum of J is obtained from (Kwakernaak and Sivan, 1972; Anderson and Moore, 1990)

$$f_T = -G_c z \quad (4.8)$$

where

$$G_c = \frac{1}{r} B^T P \quad (4.9)$$

in which P is the solution of algebraic Riccati equation

$$PA + A^T P - \frac{1}{r} P B B^T P + Q = 0 \quad (4.10)$$

In the case of the rail-counterweight system, the matrix A is actually not constant during the vibration of the counterweight. For the purpose of obtaining the control force, however, the original value of A related to the non-contact condition is used in (4.10). Because of the limited space available for actuator, the control force for the rail-counterweight system is limited to 400 lb, slightly less than 10% of its total weight, representing a small actuator.

The weight matrix Q is chosen to be $Q_{11} = 1$ and zero for other elements, implying that the lateral displacement of the counterweight is of primary concern. Several values of weight factor r are used in the analyses to obtain the best result for the system. Lower value of r produces higher control force, and vice versa. The optimal values of r for mass ratio μ of 10%, 20%, and 30% are found to be 2×10^{-6} , 3.5×10^{-6} , and 2×10^{-5} , respectively.

Next we show the numerical results obtained for the elevator counterweight system used in previous numerical studies, but now installed with an active system. Figures 4.1 and 4.2 show the ratio of maximum stress in the rail as a function of frequency ratio of mass damper

under actual Northridge and El Centro earthquakes, respectively. It is noted that there are significant reductions in the maximum stress with the implementation of this active control approach. The range of frequency ratio over which the active control is effective in reducing the response is broader than the frequency range in the passive case. For both excitations, the smaller mass ratio is seen to perform better than the larger ones. For the El Centro earthquake, the 10% and 20% mass damper produce similar results in the frequency ratio between 0.8 and 1.1. This happens because the stress due to the in-plane motion has been reduced significantly so that the stress due to the out-of-plane motion controls the maximum stress in the rail.

Numerical results also show that only TMD with mass ratio of 10% and 20% perform significantly better than the passive scheme. The TMDs with higher mass ratios do not improve much with this active control method. One of the reasons is probably the low control force shown in Figures 4.3 and 4.4 is not enough to drive the larger mass. This low control force is the result of the high weight factor r compared to the smaller mass as mentioned above. Attempting to reduce the weight factor does increase the control force but this was seen to make it even worse than the passive case.

The maximum displacement of mass damper is shown in Figures 4.5 and 4.6. Similar to the passive case, for frequency ratio higher than 0.8 the maximum displacement of the mass damper is acceptably low to be accommodated within the physical dimensions of the system.

Next we show the results for an ensemble of synthetic ground motions with similar frequency characteristics in Figures 4.7 to 4.9. Similar trend as in the previous set of figures can be observed in these figures. The mean plus one standard deviation of peak stress is significantly reduced by the active control approach. Again, the damper with small mass ratio (10%) performs better than those with higher mass ratio, especially for the high intensity

ground motions. The maximum control forces needed to achieve these results are shown in Figure 4.8. It is noted that the maximum value of the control force does reach the maximum capacity of the actuator (400 lbs), thus saturating the actuator.

The overall effectiveness of the control system can be again measured in terms of the reduction in the system fragility caused by the control scheme. Figure 4.9 shows fragility curves of the system for dampers with two mass ratios. The fragility curves of the uncontrolled system as well as those of the passive systems with two mass ratios are shown. The figures clearly show the improvements in the seismic performance of the system measure by the reductions it causes in the probability of failure of the system as a function of the ground motion intensity.

4.3 Acceleration-feedback Approach

As mentioned earlier, the sensors for the measurement of full system state may be difficult to install. It is, however, easy to measure accelerations by placing accelerometers at specific locations on the structure. The accelerometer measures absolute acceleration at a point, thus, unlike state vector that contains relative displacement and velocity, the measurement is independent of reference frame of the structure. However, the measured accelerations must be converted to the system state, which is needed for calculating the control force. This requires the use of an observer system, and a somewhat different feedback control algorithm. In this section, this acceleration-feedback control approach for the rail-counterweight system will be discussed.

The absolute acceleration of the three degrees-of freedom of the rail-counterweight system with mass damper can be measured by placing three accelerometers, one at the center

of mass of the counterweight, one at the lower end of the frame, and one at the mass damper. Analytically, the absolute acceleration measurement is given by

$$\mathbf{y}_m = \mathbf{C}_y \mathbf{z} + \mathbf{D}_y f_T + \mathbf{M}_i^{-1} \mathbf{f}_i + \mathbf{v} \quad (4.11)$$

where

$$\mathbf{C}_y = \begin{bmatrix} -\mathbf{M}_i^{-1} \mathbf{K}_i & -\mathbf{M}_i^{-1} \mathbf{C}_i \end{bmatrix} \quad ; \quad \mathbf{D}_y = \mathbf{M}_i^{-1} \mathbf{D} \quad (4.12)$$

and \mathbf{v} is a vector of measurement noise.

The LQG (Linear Quadratic Gaussian) method is used to obtain the control action based on this acceleration feedback. Again, this is a control algorithm for a linear system with quadratic performance index (equation (4.7)), with the measurement noise assumed to be Gaussian white noise process (Kwakernaak and Sivan, 1972, Anderson and Moore, 1990). For the rail-counterweight system, the acceleration inputs are also assumed to be Gaussian with ratio of intensity γ with respect to the measurement noise.

Using the LQG method, the state vector is estimated by the estimator, which is a part of the controller, using the measured acceleration feedback (Kwakernaak and Sivan, 1972)

$$\dot{\hat{\mathbf{z}}} = \mathbf{A} \hat{\mathbf{z}} + \mathbf{B} f_T + \mathbf{G}_e (\mathbf{y}_m - \mathbf{C}_y \hat{\mathbf{z}} - \mathbf{D}_y f_T) \quad (4.13)$$

or

$$\dot{\hat{\mathbf{z}}} = (\mathbf{A} - \mathbf{G}_e \mathbf{C}_y) \hat{\mathbf{z}} + (\mathbf{B} - \mathbf{G}_e \mathbf{D}_y) f_T + \mathbf{G}_e \mathbf{y}_m \quad (4.14)$$

In equation (4.13), the first two terms on the right-hand side represent the model of the system that is known to the estimator, and the third term corrects the model by amplifying the difference between the computed output and the measured output with estimator gain \mathbf{G}_e . This estimator gain matrix is obtained from

$$\mathbf{G}_e = \mathbf{S}_e \mathbf{C}_y^T \quad (4.15)$$

where S_e is the solution of the algebraic Riccati equation

$$AS_e + S_eA^T - S_eC_y^TC_yS_e + \gamma EE^T = 0 \quad (4.16)$$

The control force is then calculated from the estimated state

$$f_T = -G_c \hat{z} \quad (4.17)$$

where G_c is the full state feedback gain matrix, the same gain matrix that was obtained from the LQR algorithm in the previous section.

In the numerical analysis, the intensity of the measurement noise is assumed to be 4% of the intensity of the input, so that $\gamma = 25$. Other parameters, such as constant value of matrix A in determining the gain matrices and the saturation limit of the control force, are the same as in the previous section. Several values of weight matrix Q and weight factor r were used to obtain the best result. The results presented here are obtained using $Q_{11} = Q_{22} = Q_{33} = Q_{44} = 1$ and zero elsewhere and $r = 5 \times 10^{-6}$.

To obtain the numerical results, the rail-counterweight system considered for the previous numerical results is considered again. Figures 4.10 and 4.11 show the ratio of maximum stress in the rail as a function of the frequency ratio of mass damper under actual Northridge and El Centro earthquakes, respectively. The results of passive TMD are also plotted in those figures for comparison. Under Northridge earthquake, the active method with acceleration feedback improves the passive TMD when the frequency ratio is 0.9 or higher. As much as 25% reduction in the maximum stress in the rail is achieved by the system with 20% mass damper ratio. Similar trend is also observed for the El Centro earthquake, although now the 10% mass damper ratio performs better. These observations are also confirmed by the results under an ensemble of synthetic ground motions, presented in Figure 4.12 in terms

of maximum values of mean plus one standard deviation of the peak stress. In general, the active control is seen to improve the performance of the mass damper. The acceleration feedback results are, however, not as good as the results for the full state feedback simply because some assumptions are made in estimating the full state from the measured accelerations. The 10% mass damper performs slightly better under low to medium earthquakes and the 20% mass damper is slightly better under strong earthquake. However, in terms of fragility, where the maximum stress at every possible location of counterweight contributes to the probability of failure, the 20% mass damper performs better (Figure 4.13). The mean and maximum values of peak control force are plotted in Figure 4.14. It is noted that the response improvement can be achieved with quite a low control force.

4.4 Semi-active Approach

Semi-active control devices combine the benefits of passive control device with the ability to adapt to the response of the structure. Moreover, the power requirement for this type of devices is much lower than that of the active control devices. The semi-active devices do not input energy into the system. The capability to adjust the control force is implemented by changing the properties of the device, such as stiffness or damping values. The energy dissipation is usually provided by surface friction or viscous or viscoelastic-plastic fluids within the devices.

MR Dampers

In automotive vibration isolation designs and civil engineering applications, the use of the Magnetorheological (MR) devices called MR-damper has attracted special attentions of researchers and designers. The MR dampers are preferred because of their fast response and stable force deformation characteristics. They use special fluids with suspended magnetic

particles which can be charged to change the viscosity of the fluid drastically almost instantaneously. The damper fluid properties are thus highly controllable. The MR damper consists of a main cylinder that houses the piston and accumulator and is filled with MR fluid. A magnetic circuit is attached to the piston head. A schematic of this MR damper is shown in Figure 4.15. The MR fluid is the magnetic analog of the electrorheological (ER) fluid. When a magnetic field is applied to the fluid in the damper, the fluid becomes semi-solid and exhibits plastic behavior similar to the ER fluid. The advantages of MR fluid include high yield strength, changeable viscosity, and stable hysteretic behavior over a broader temperature range (Dyke et al., 1996; Spencer et al., 1997).

Force Deformation Model of MR Damper

Spencer et al. (1997) proposed a simple mechanical model for the MR damper. This model, shown in Figure 4.16, has been shown to predict the behavior of the MR damper accurately. From this model, the force in the damper can be defined in terms of the equations

$$f = \alpha z + c_o (\dot{x} - \dot{y}) + k_o (x - y) + k_l (x - x_o) \quad (4.18)$$

$$f = c_l \dot{y} + k_l (x - x_o) \quad (4.19)$$

where c_o , c_l , k_o , and k_l are the coefficient of damper and spring as shown in Figure 4.16, x and y are the degrees-of-freedom of the damper, also shown in the same figure, z is the evolutionary variable of the Bouc-Wen element, and α is the coefficient for the Bouc-Wen's evolutionary variable z . When attached to the mass damper of the rail-counterweight system, x represents the displacement of the mass damper relative to the frame of the counterweight.

The evolutionary variable z of the Bouc-Wen element is governed by

$$\dot{z} = -\gamma |\dot{x} - \dot{y}| z |z|^{n-1} - \beta (\dot{x} - \dot{y}) |z|^n + A (\dot{x} - \dot{y}) \quad (4.20)$$

where γ , β , A , and n are the Bouc-Wen model parameters whose values control the shape of the hysteresis loops for the element.

Using equations (4.18) and (4.19), we obtain the following equation for the degree-of-freedom y :

$$\dot{y} = \frac{1}{c_o + c_1} [\alpha z + c_o \dot{x} + k_o (x - y)] \quad (4.21)$$

Spencer et al (1997) suggested the dependence of the force on the applied voltage through the linear relationship between the dashpots and the Bouc-Wen element in the mechanical model and the applied voltage:

$$\alpha = \alpha_a + \alpha_b u \quad (4.22)$$

$$c_o = c_{oa} + c_{ob} u \quad (4.23)$$

$$c_1 = c_{1a} + c_{1b} u \quad (4.24)$$

where u is the output of the first order filter for the commanded voltage v :

$$\dot{u} = -\eta(u - v) \quad (4.25)$$

The force-deformation diagram for this mechanical model under 2.5 Hz sinusoidal excitation is shown in Figure 4.17 for different level of voltage. Figure 4.18 shows the force-velocity relationship under the same excitation. These results are generated using the parameters obtained by Dyke et al. (1996) from fitting the generalized analytical model with the experimental results of a prototype MR damper. At zero voltage, the model appears to behave like a viscous device with approximately elliptical force-deformation and almost linear force-velocity relationships. With increasing voltage, the force increases and the model behaves like a plastic material in parallel with viscous damper.

State Equations of the System with MR Dampers

To solve the equations of motion of the rail-counterweight system with mass damper and MR damper device, equations (4.20), (4.21), and (4.25) are added to the original equations of motion (4.4), where the control force f_T is now replaced by the force from the MR damper shown in equation (4.18) or (4.19). The complete set of equations of motion becomes:

$$\dot{z} = \mathbf{A}z + \mathbf{B}f_T + \mathbf{E}\ddot{x} + \mathbf{f}^* \quad (4.26)$$

$$\dot{z} = -\gamma|\dot{x} - \dot{y}|z|z|^{n-1} - \beta(\dot{x} - \dot{y})|z|^n + A(\dot{x} - \dot{y}) \quad (4.27)$$

$$\dot{y} = \frac{1}{c_o + c_1} [\alpha z + c_o \dot{x} + k_o(x - y)] \quad (4.28)$$

$$\dot{u} = -\eta(u - v) \quad (4.29)$$

In this study, the parameters defined by Dyke et al (1996) for a prototype MR damper with 3000 N (674 lbs) maximum force are used. The force range and the size of the device (3.8 cm diameter, 21.5 cm extended length, and ± 2.5 cm stroke) make quite suitable for use on a rail-counterweight system. The maximum voltage for this MR damper is 2.25 V as the saturation effect begins at voltage higher than 2.25 V (Dyke et al., 1996).

Control Procedure Implementation

The acceleration-feedback control algorithm discussed in the previous section is used to determine the required control force. The control force, however, cannot be regulated directly by the MR damper. It can only command the voltage that will be applied to the current driver. Spencer and Dyke et al (1996, 1997) used the clipped-optimal control algorithm to select the appropriate voltage. In this scheme, the required control force is compared to the measured force at the MR damper. If the magnitude of the required force is more than measured force,

and both are in the same direction, the maximum voltage is applied. If both have the same value, the voltage stays at the present level. In other cases the voltage is turned off. This approach is also used for the MR damper in this study.

Tables 4.1 to 4.4 present the maximum stress in the rail using different response control methods and the percentage of stress reduction from the uncontrolled system. Tables 4.1 and 4.3 are for actual El Centro earthquake (0.348g) and Tables 4.2 and 4.3 are for actual Northridge earthquake (0.843g). The mass damper is 10% of the total mass of the counterweight for Tables 4.1 and 4.2, and 20% for Tables 4.3 and 4.4. The frequency ratio of the mass damper system is fixed at 0.9 in all of these results. The active control results are from the acceleration-feedback control algorithm. Since MR damper can also be used as passive damper, the results are also included for comparisons. In these passive schemes, the voltage remains constant during vibrations, either turned off (0 V) or always on (2.25 V).

All four tables show that using semi-active scheme with MR damper device can reduce the maximum stress in the rail with comparable results to the active approach. For El Centro earthquake, the semi-active method gives the best results while for Northridge earthquake it gives close results to the active control. It should also be mentioned that operating MR damper in semi-active mode could produce better results than using maximum voltage (passive-on) during the whole vibration.

The results of fragility analysis using an ensemble of synthetic ground motions are shown in Figures 4.19 to 4.21. Here the results from the three control schemes, i.e. passive tuned mass damper, active mass damper using acceleration-feedback, and semi-active with MR damper using acceleration feedback, are compared for the system with 10% mass ratio and frequency ratio 0.9. Figure 4.19 shows the mean plus one standard deviation of the peak

stress in the rail and Figure 4.20 presents the fragility curves for the uncontrolled system and the three control schemes. The same fragility curves are plotted in two separate graphs in Figure 4.21 to provide better resolution in the differences under medium to strong earthquake. All these figures show that the semi-active scheme provides the best results in terms of mean plus one standard deviation of the peak stress in the rail and fragility of the rail-counterweight system.

4.5 Concluding Remarks

This chapter describes the application of three control schemes for use with the counterweight-rail systems: (1) active control methods using ideal full state-feedback with LQR algorithm, (2) a more practical acceleration-feedback with LQG algorithm and (3) a semi-active scheme with MR dampers that combines the benefit of passive and active dampers. Numerical results are presented to demonstrate their effectiveness in a seismic environment.

It is shown that all these methods can reduce the seismic response and improve the performance of rail-counterweight systems. With full state feedback approach more than 50% reduction in the maximum stress in the rail can be realized. However, because of the need to measure relative displacement and velocity of each degrees-of-freedom of the counterweight, it may be hard to apply this method. Acceleration-feedback approach which estimates the full state indirectly through measurements on the system accelerations, on the other hand, is more applicable to the rail-counterweight system. The numerical analyses show that this method can still improve the response of the system although not as much as the full state-feedback.

The semi-active approach utilizing a magnetorheological damper was considered as an alternative to the other two fully active approaches. The numerical results show that this

approach is better than, or at least as effective as, the acceleration feedback approach. This approach has a special advantage over the other fully active approach that it does not need an outside source of power. The fully active approaches, on the other hand, depend on the outside source of power to operate the actuator. In a strong earthquake the outside power may not be available to the actuator in the active system, whereas in the semi-active system the MR dampers can always be activated by a simple battery.

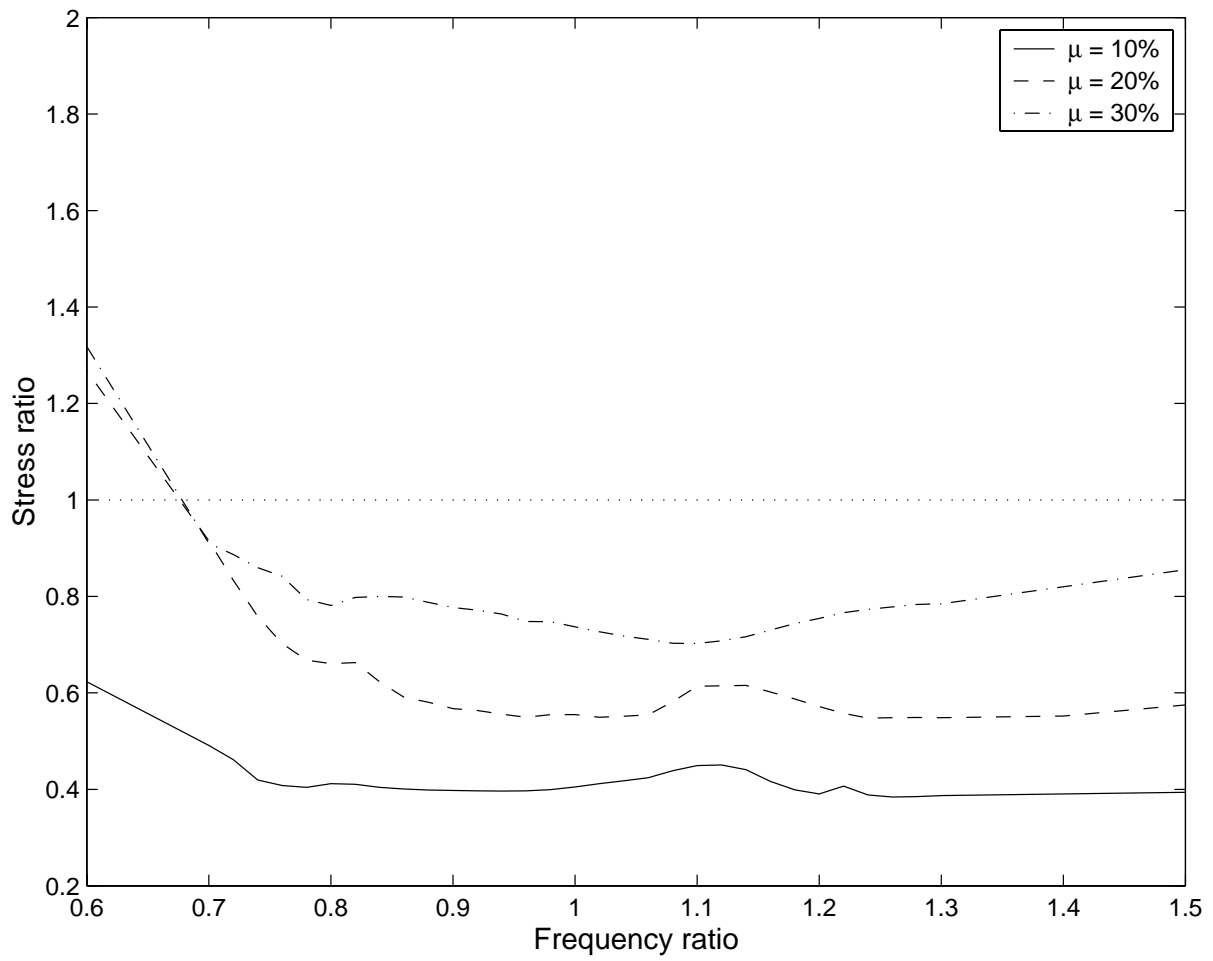


Figure 4.1 Ratio of maximum stress ratio as a function of frequency ratio under actual Northridge earthquake.

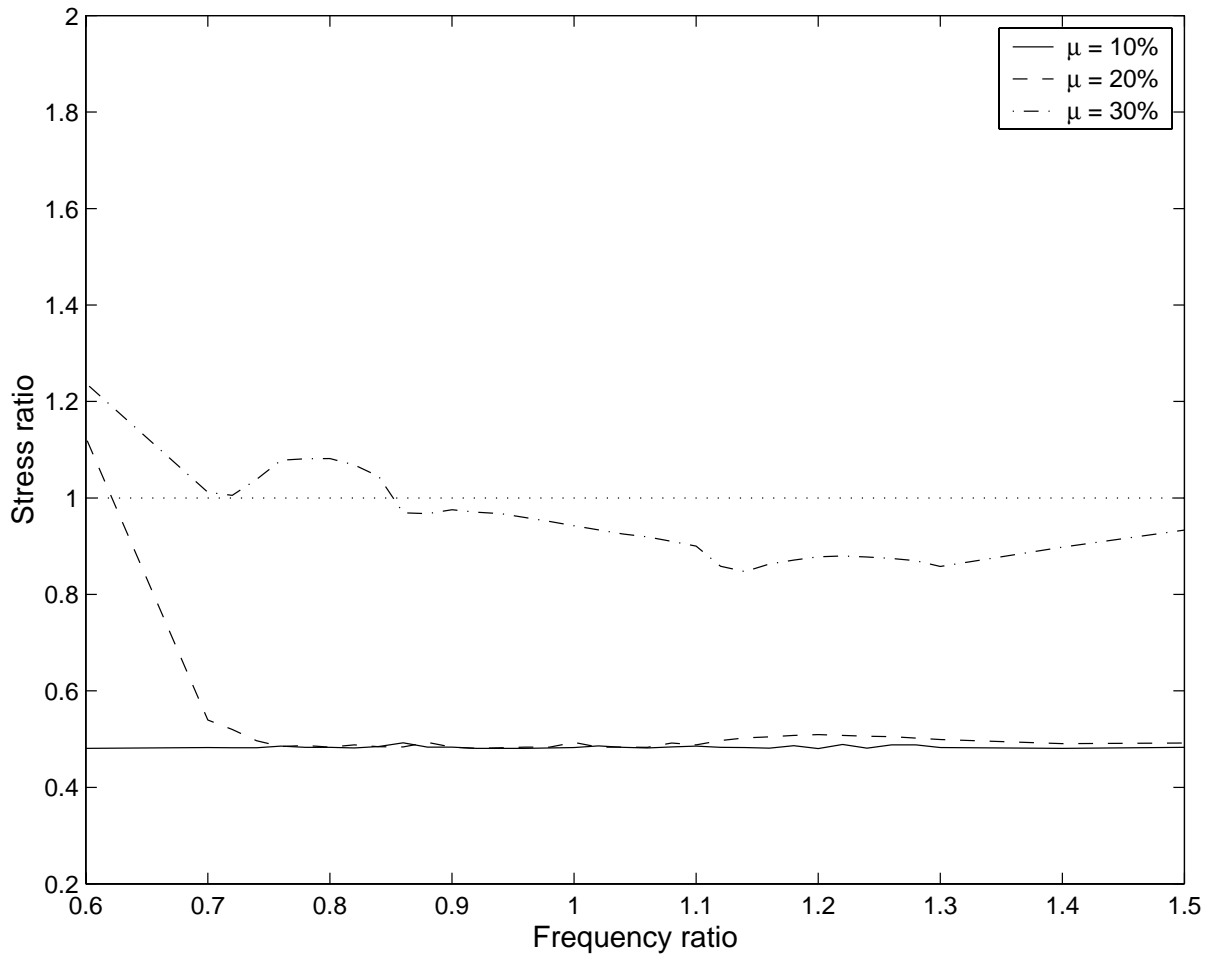


Figure 4.2 Ratio of maximum stress ratio as a function of frequency ratio under actual El Centro earthquake.

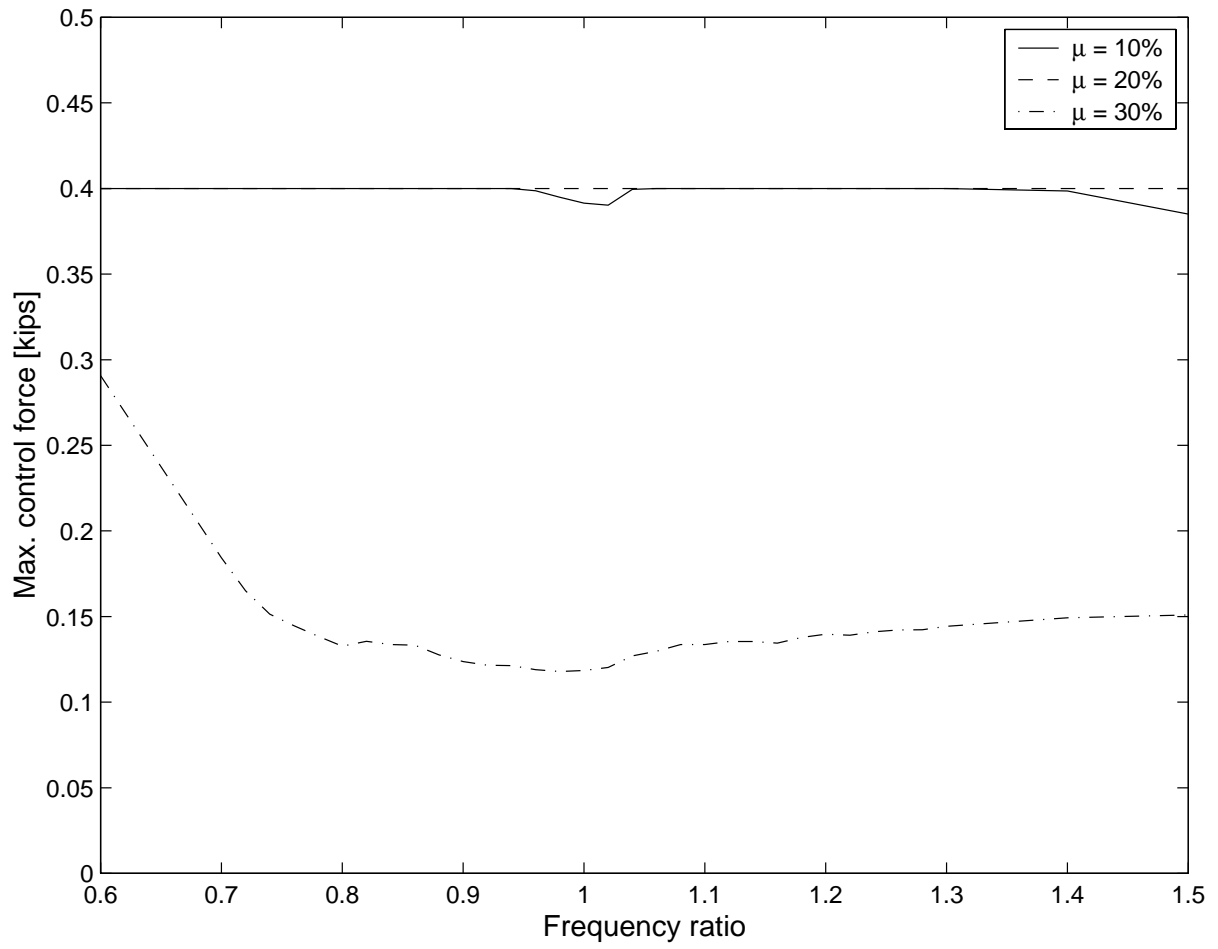


Figure 4.3 Maximum control force for actual Northridge earthquake.

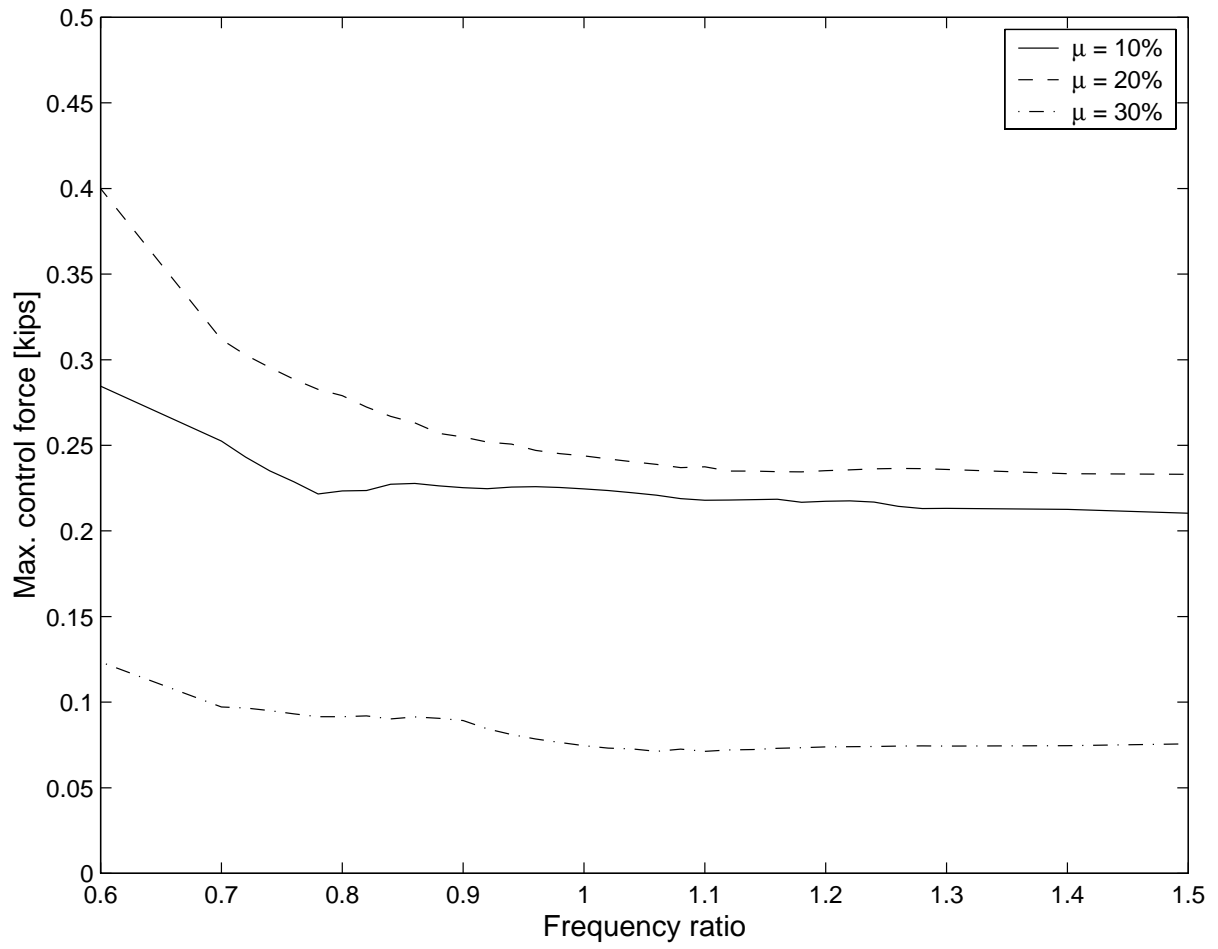


Figure 4.4 Maximum control force for actual El Centro earthquake.

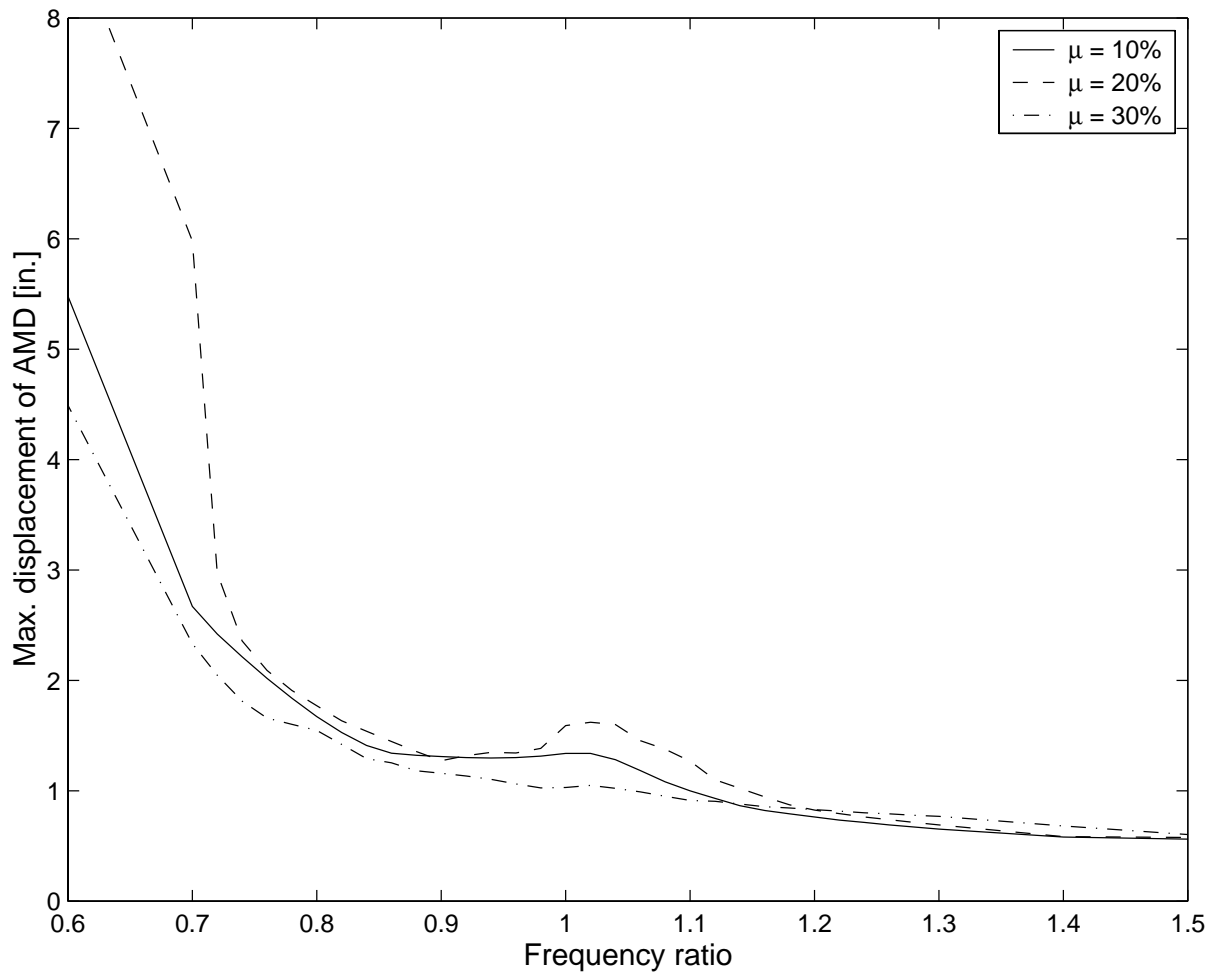


Figure 4.5 Maximum displacement of mass damper for actual Northridge earthquake.

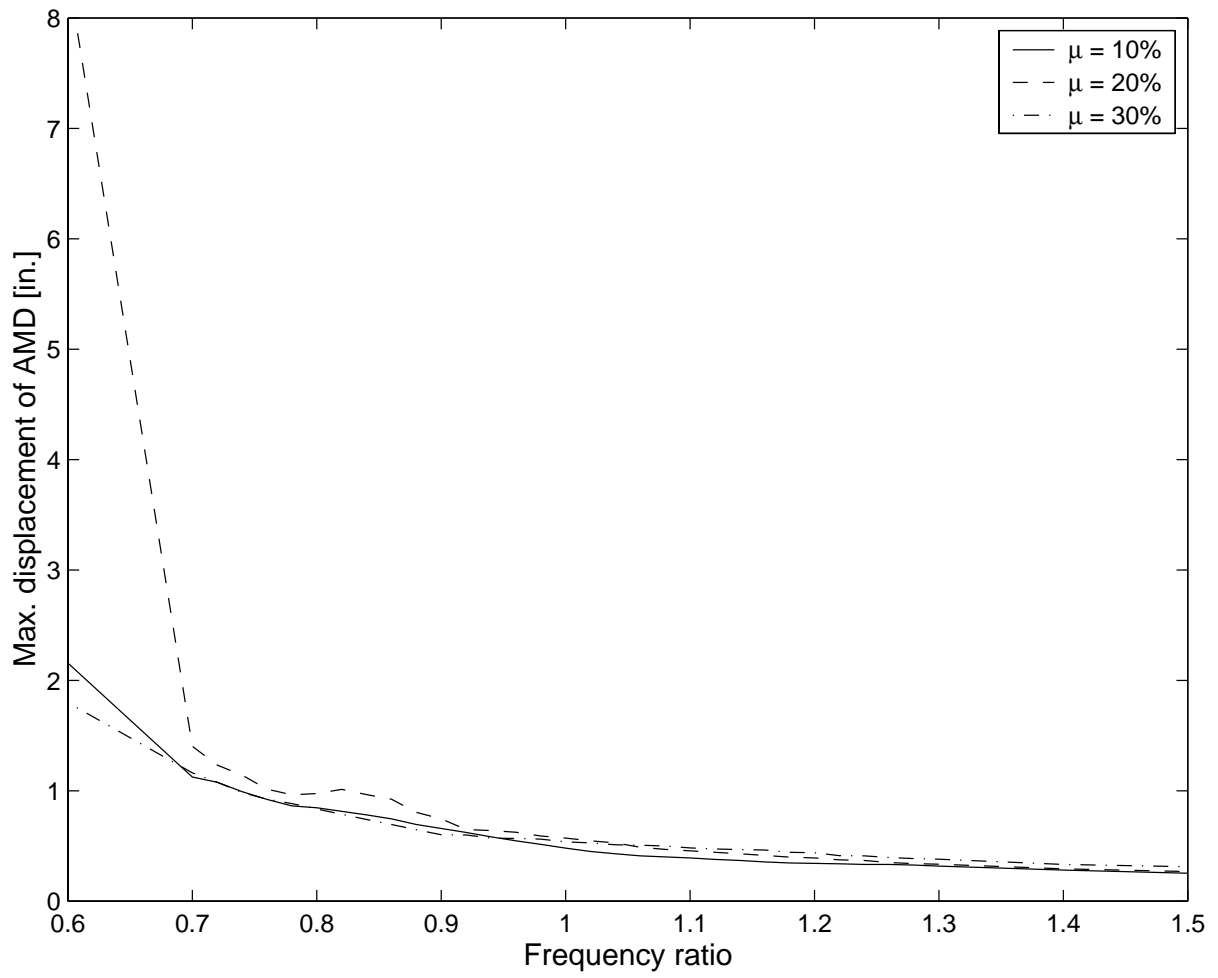


Figure 4.6 Maximum displacement of mass damper for actual El Centro earthquake.

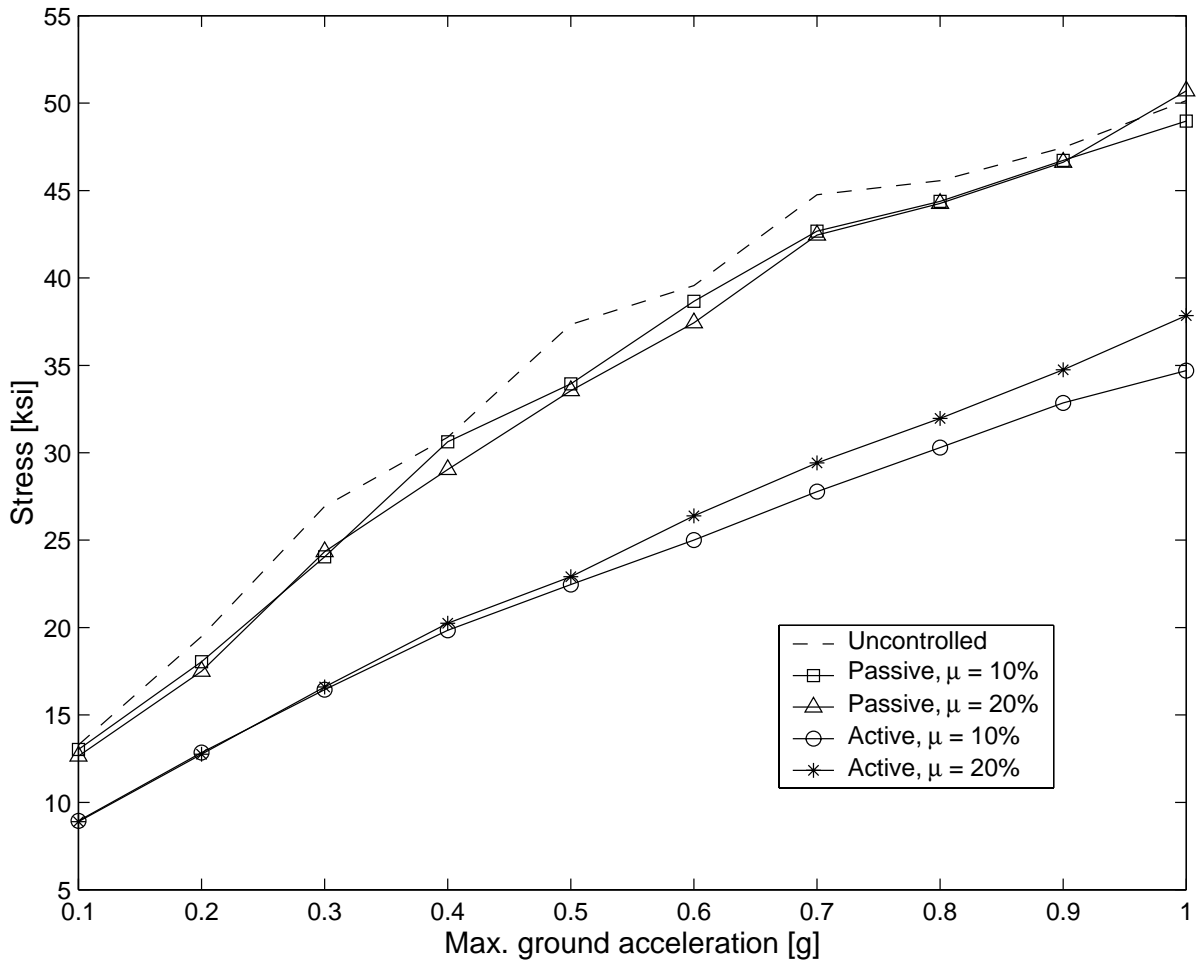


Figure 4.7 Mean plus one standard deviation of the maximum stress in the rail for an ensemble of synthetic ground motions.

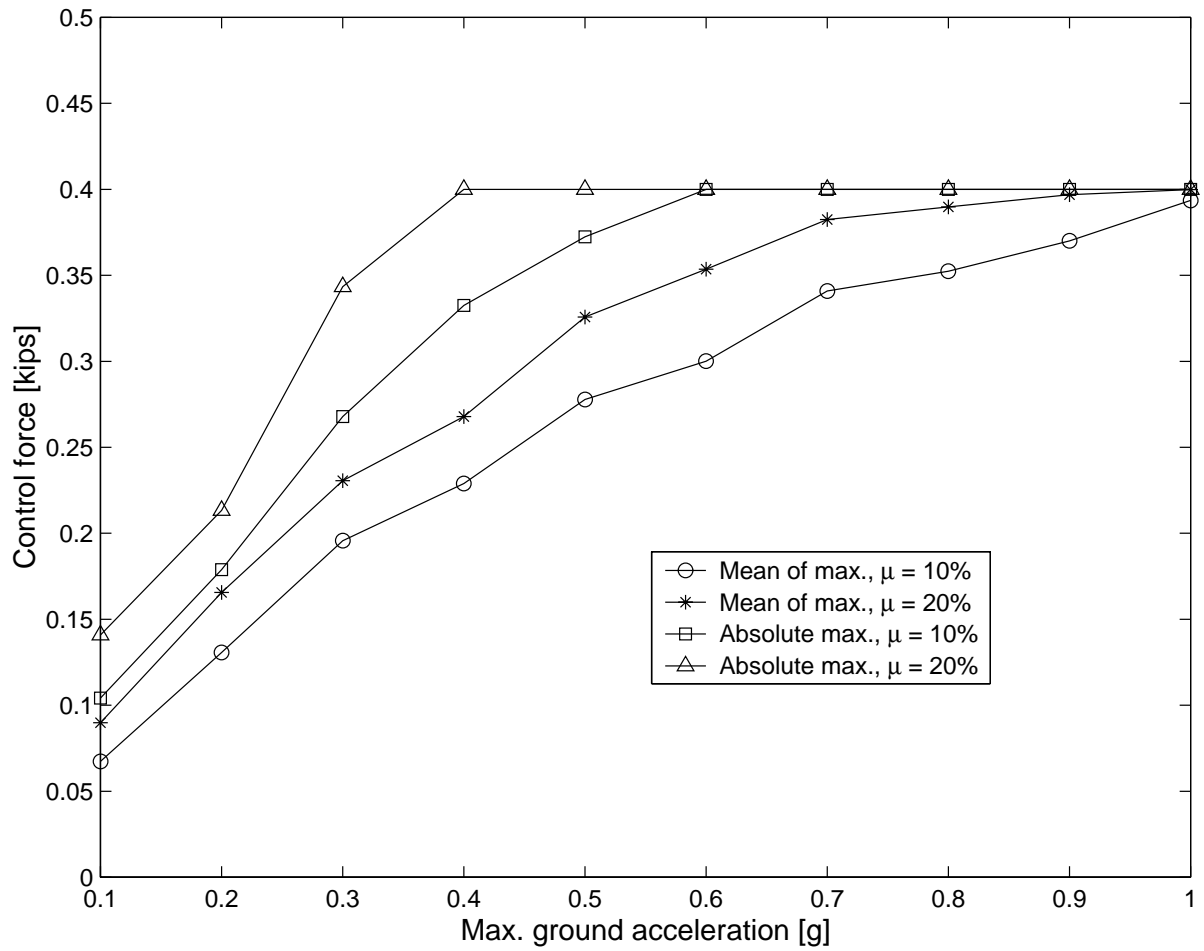


Figure 4.8 Mean and absolute maximum of peak control force under an ensemble of synthetic ground motions.

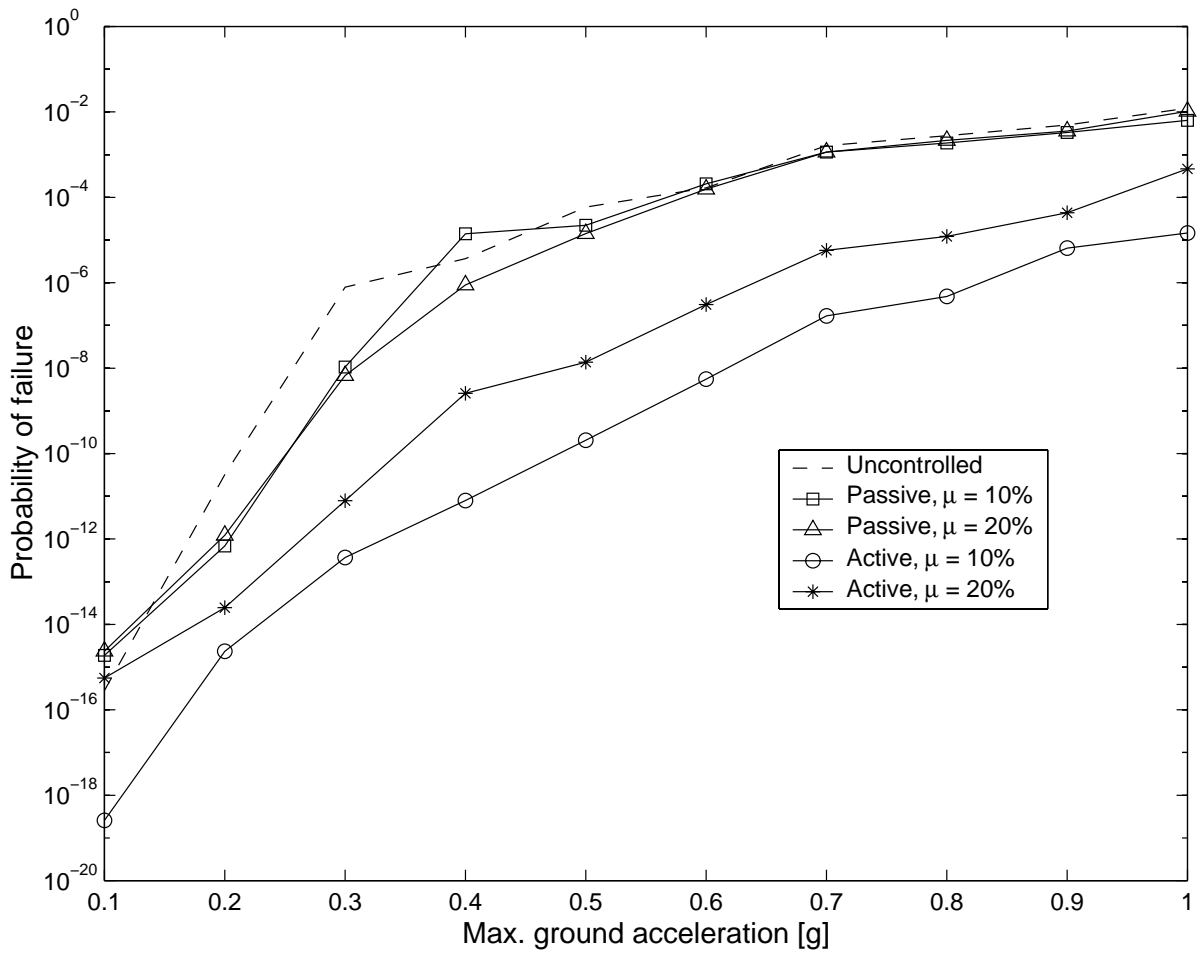


Figure 4.9 Fragility curves of the rail for passive and active control schemes.

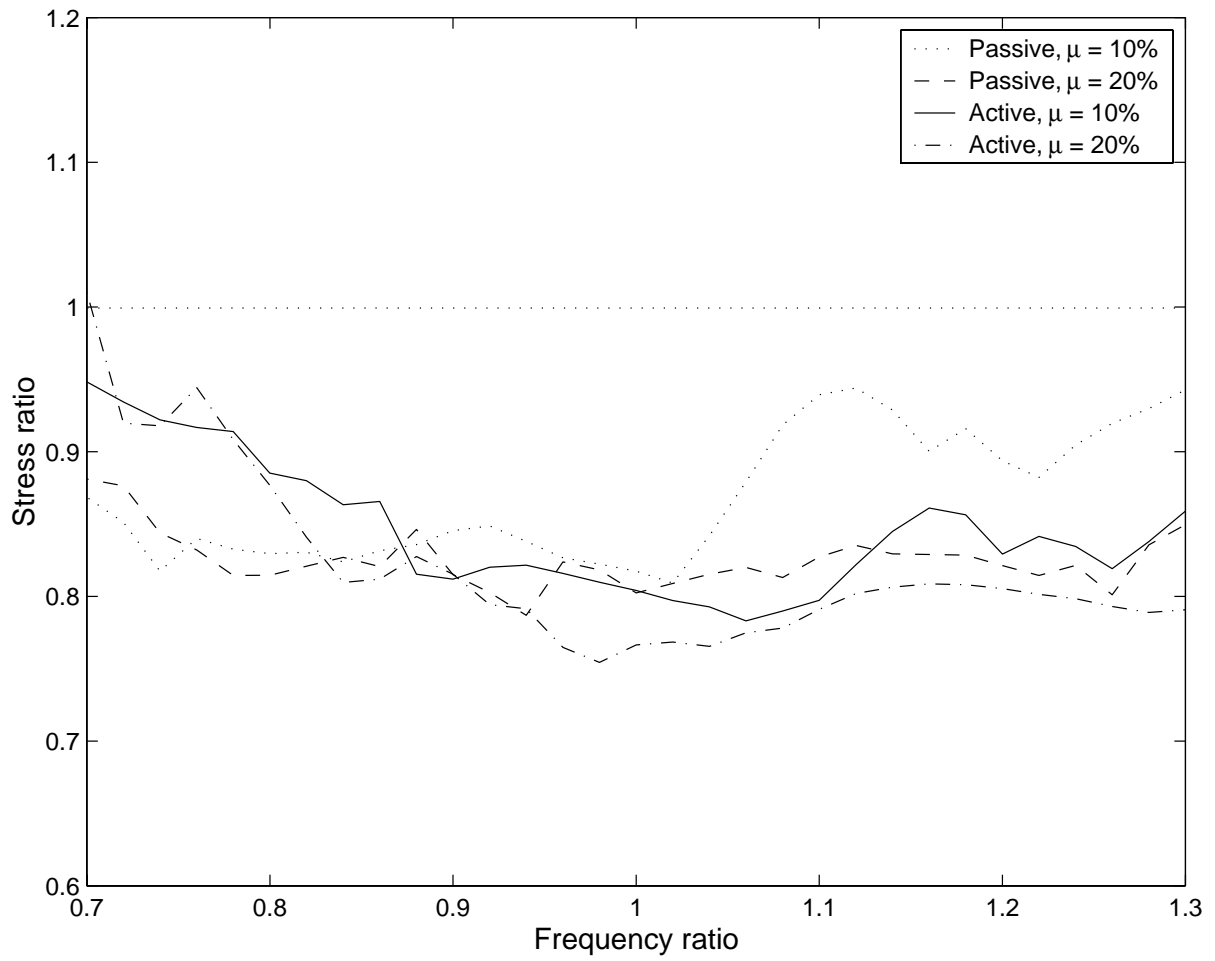


Figure 4.10 Ratio of maximum stress as a function of frequency ratio under actual Northridge earthquake.

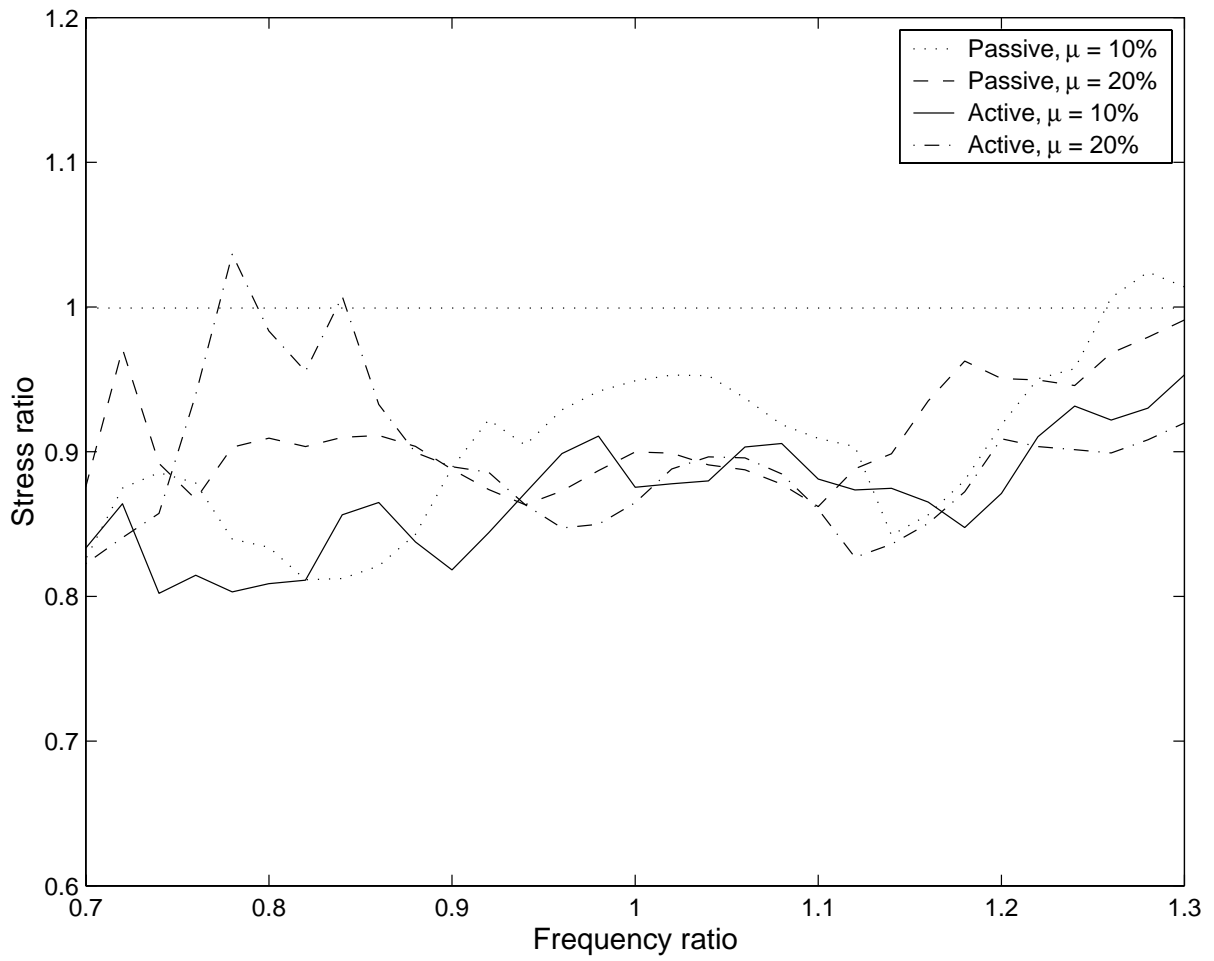


Figure 4.11 Ratio of maximum stress as a function of frequency ratio under actual El Centro earthquake.

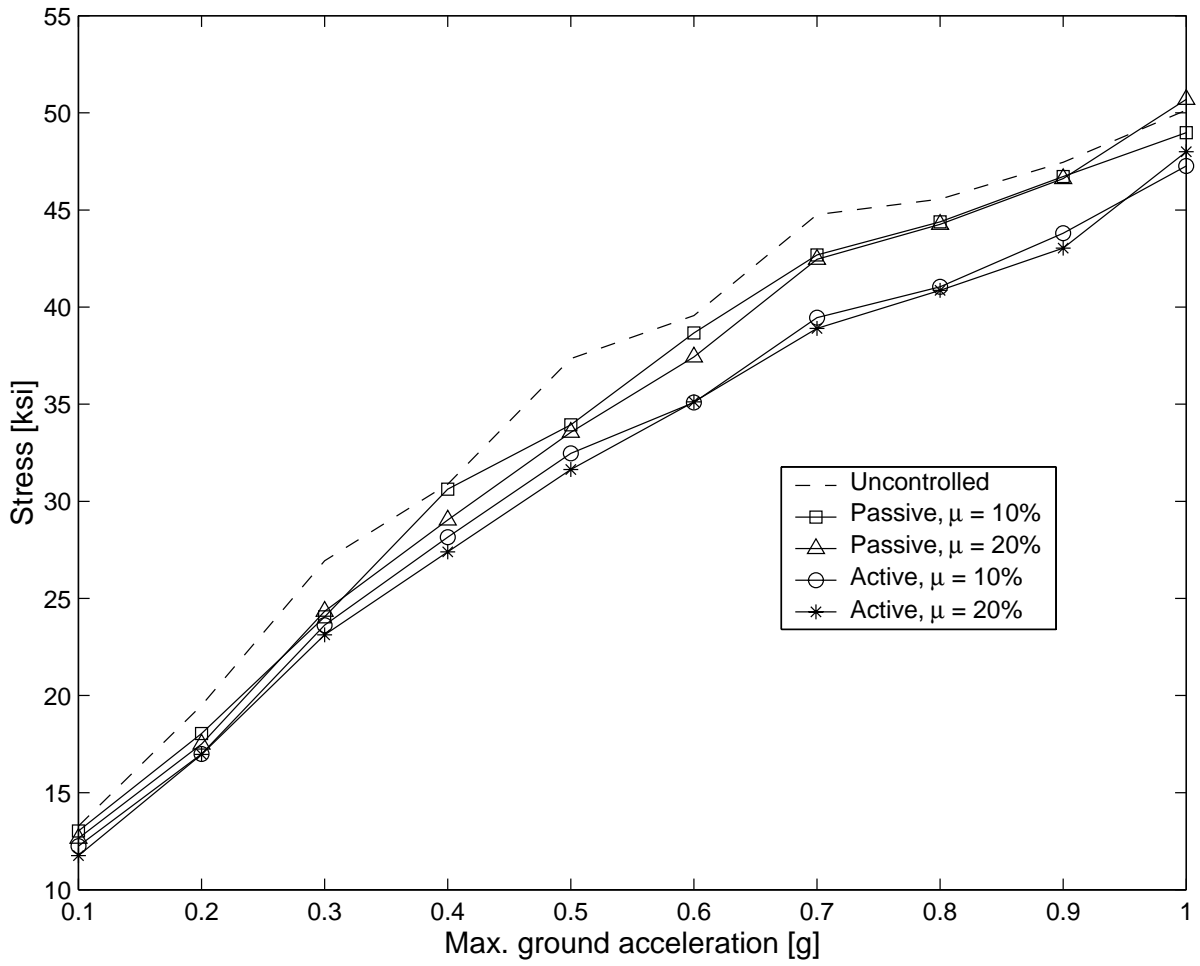


Figure 4.12 Mean plus one standard deviation of the maximum stress in the rail for an ensemble of synthetic ground motions.

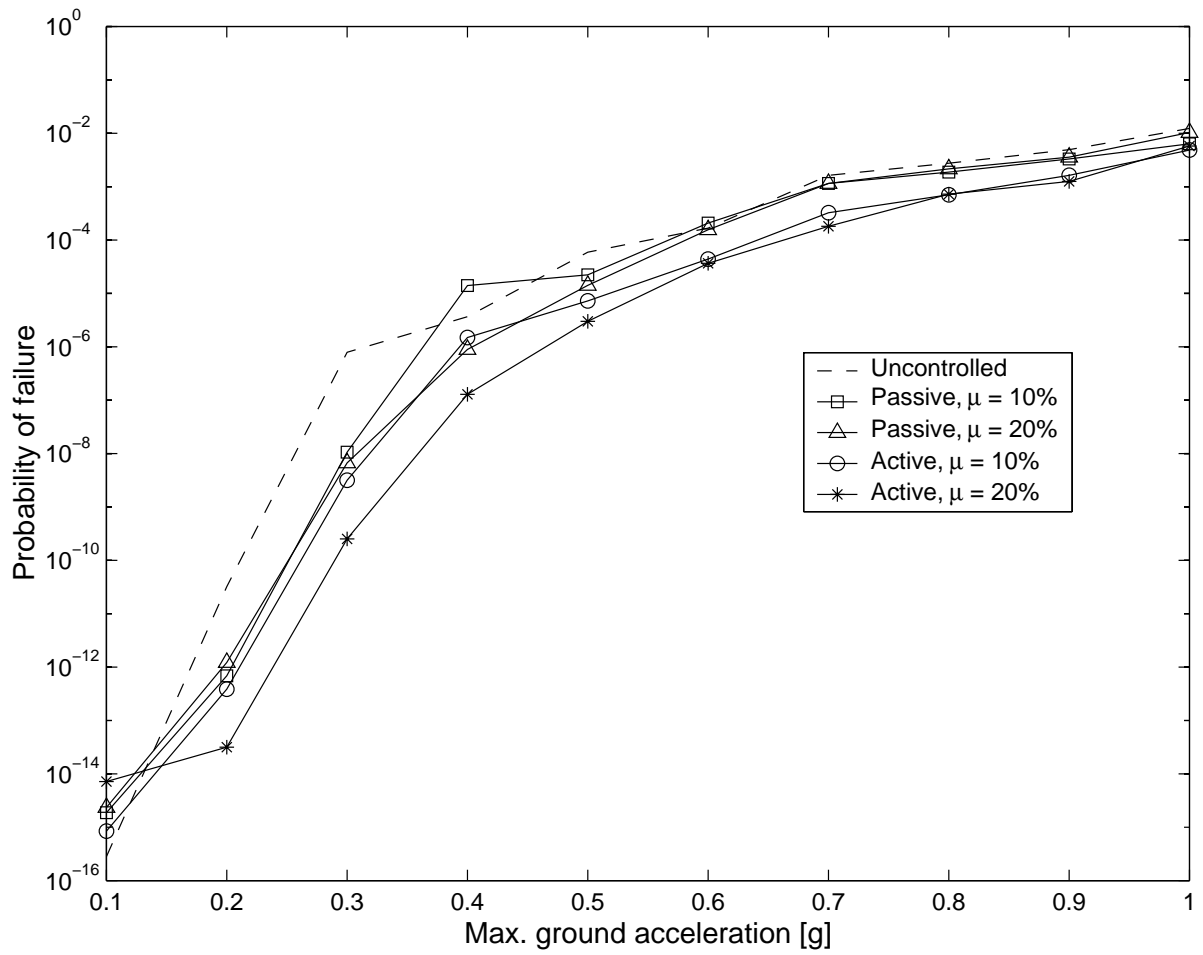


Figure 4.13 Fragility curves of the rail for passive and active control schemes.

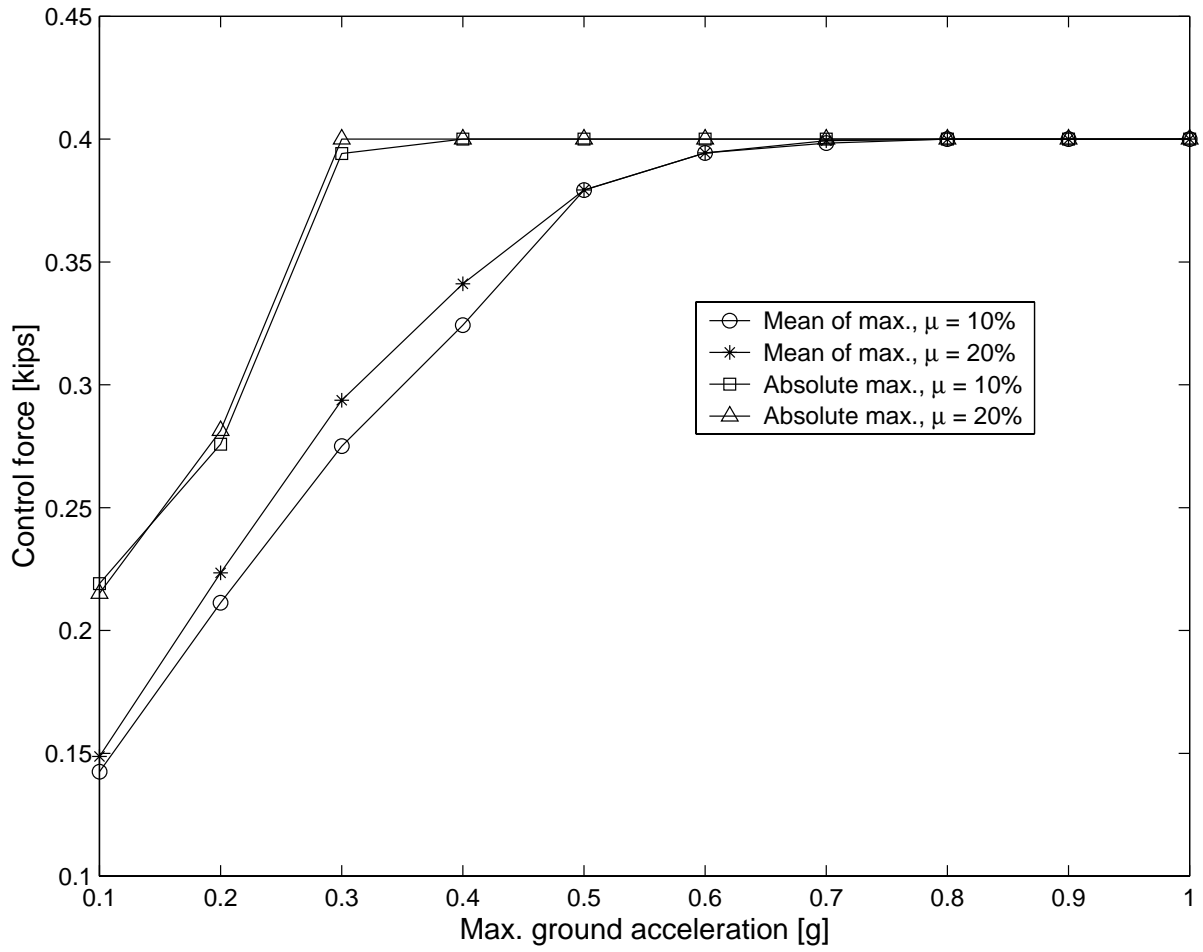


Figure 4.14 Mean and absolute maximum of peak control force under an ensemble of synthetic ground motions.

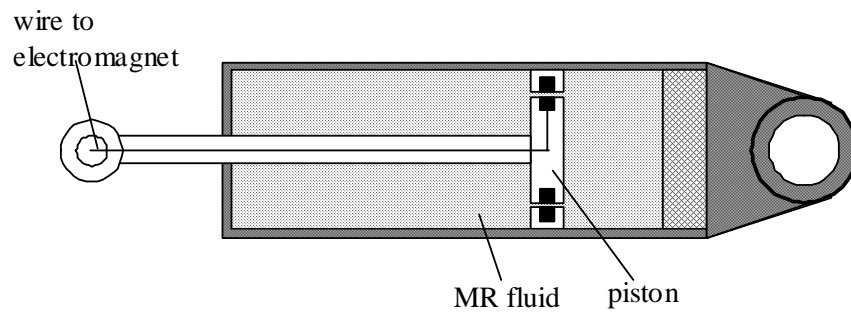


Figure 4.15 Schematic of a magnetorheological damper.

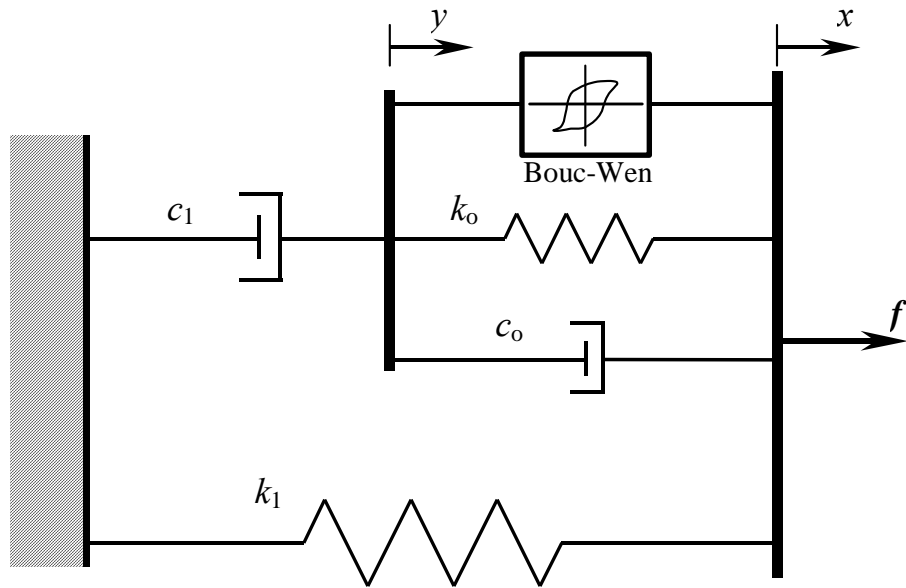


Figure 4.16 Mechanical model of MR damper as proposed by Spencer et al. (1997).

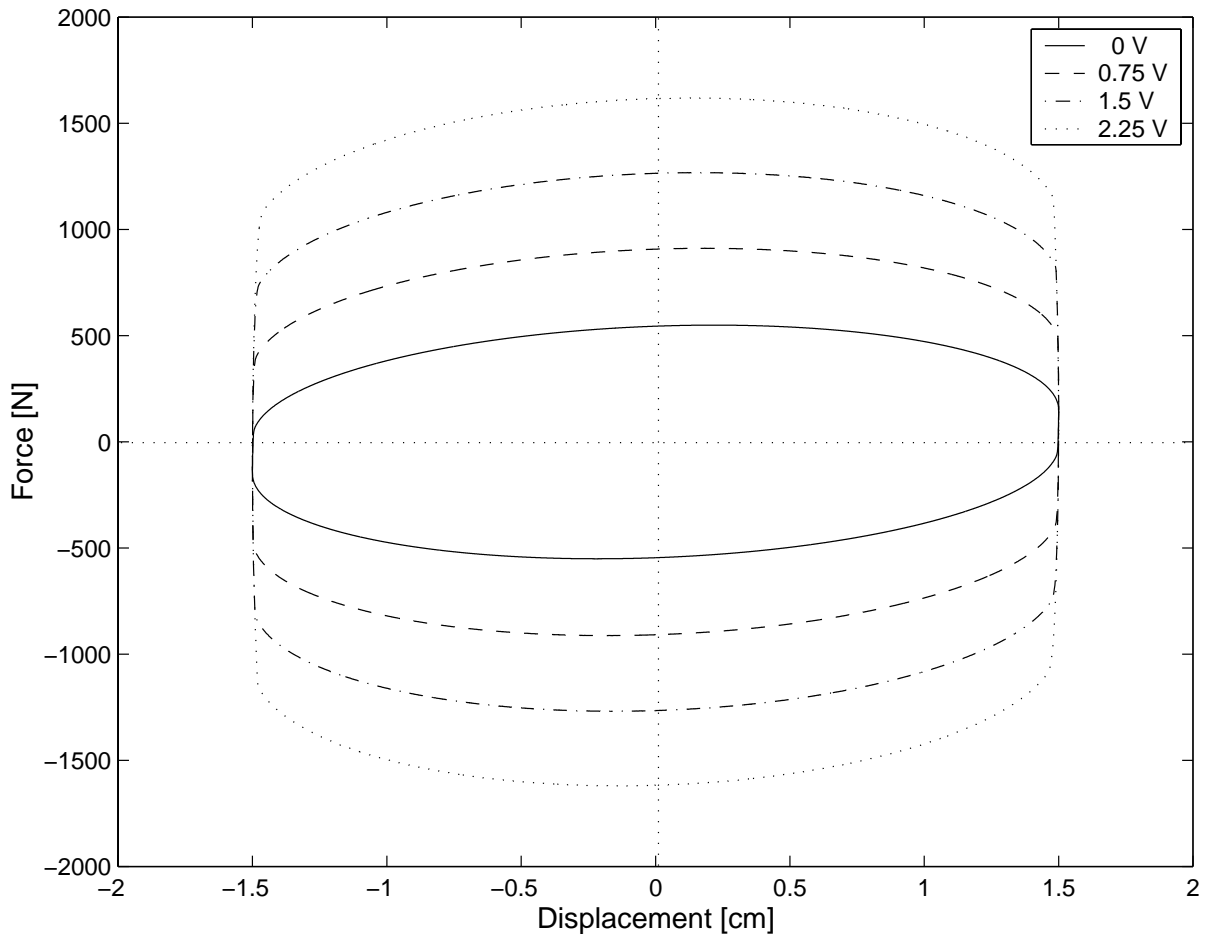


Figure 4.17 Force-displacement relationship of the mechanical model of MR damper under 2.5 Hz sinusoidal excitation for different voltage level.

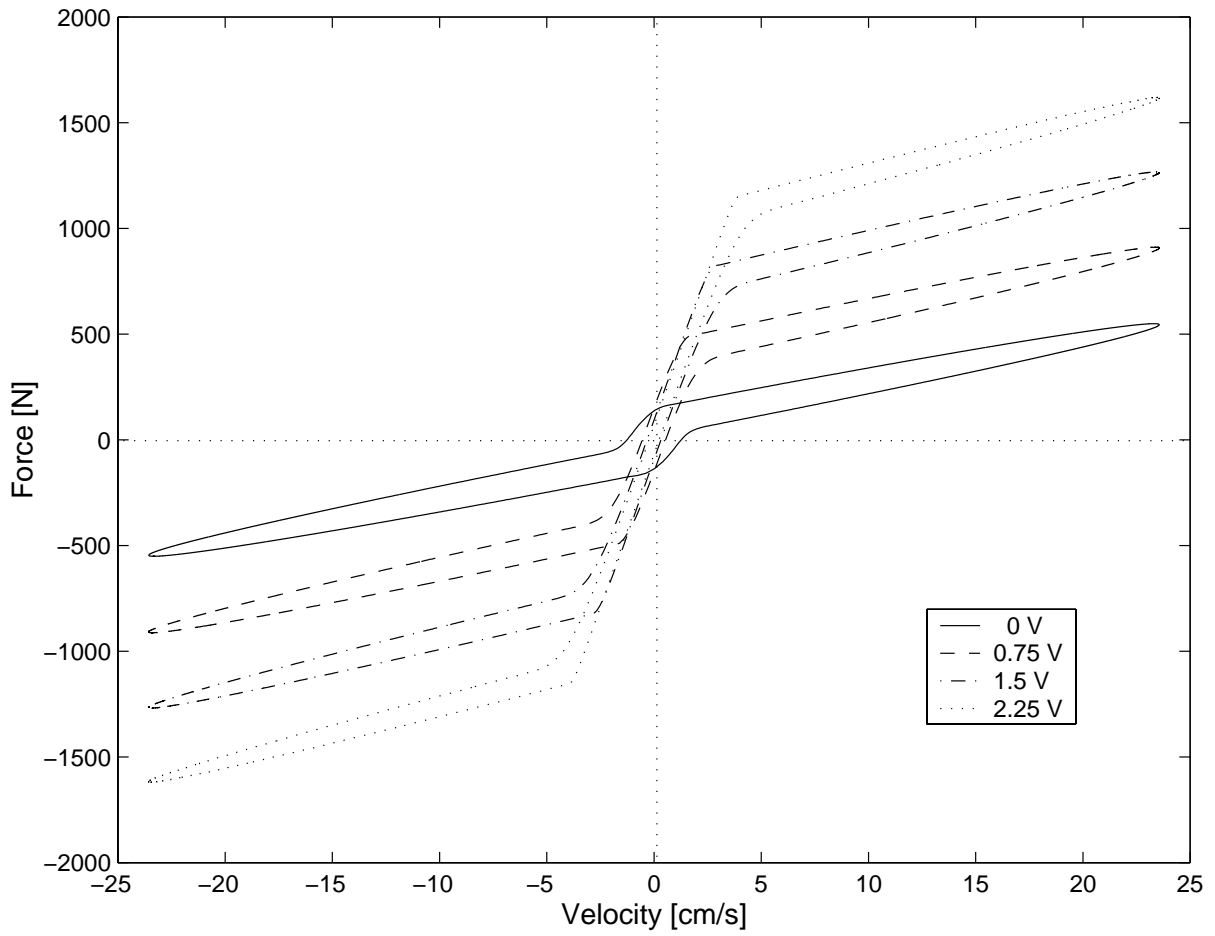


Figure 4.18 Force-velocity of the mechanical model of MR damper under 2.5 Hz sinusoidal excitation for different voltage level.

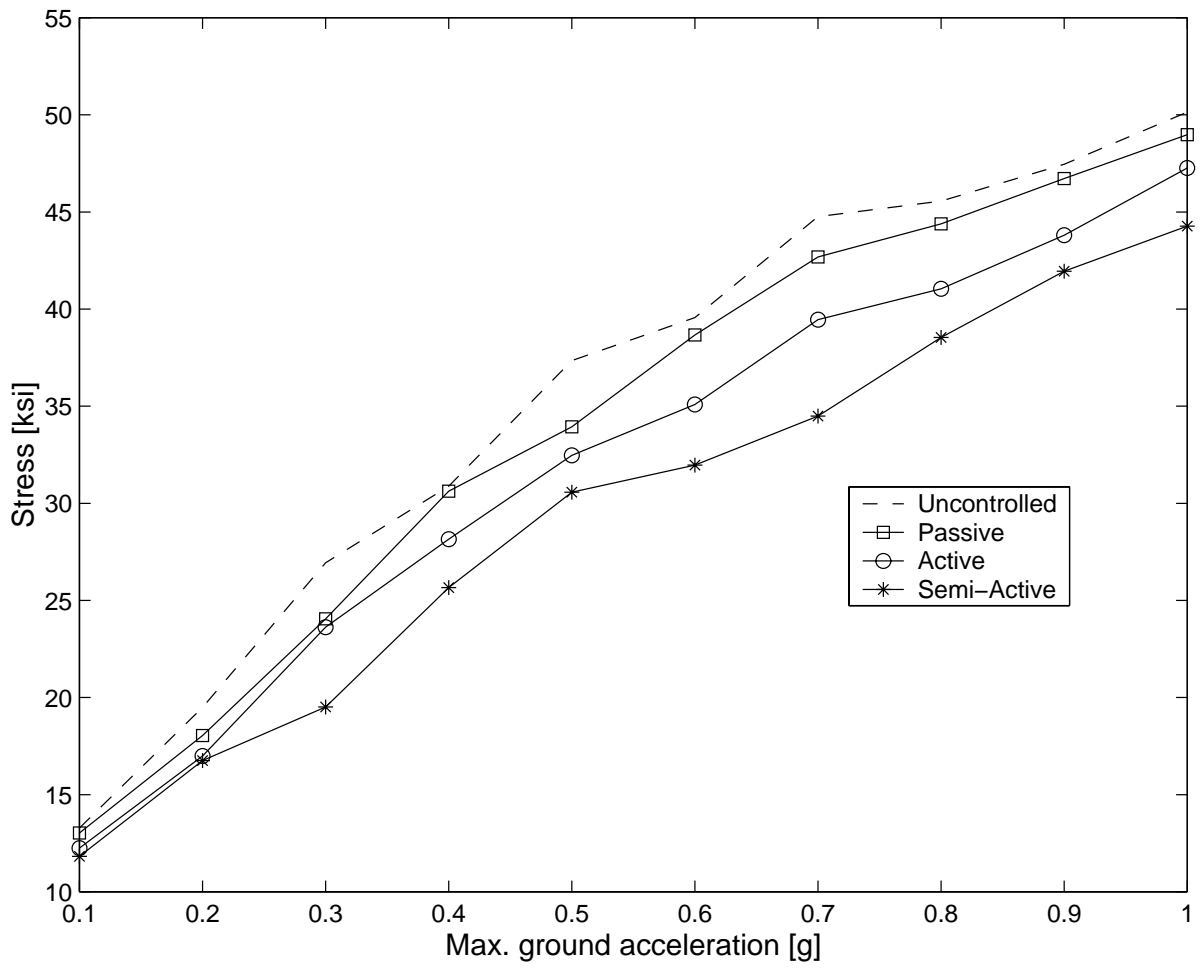


Figure 4.19 Mean plus one standard deviation of the maximum stress in the rail for an ensemble of synthetic ground motions.

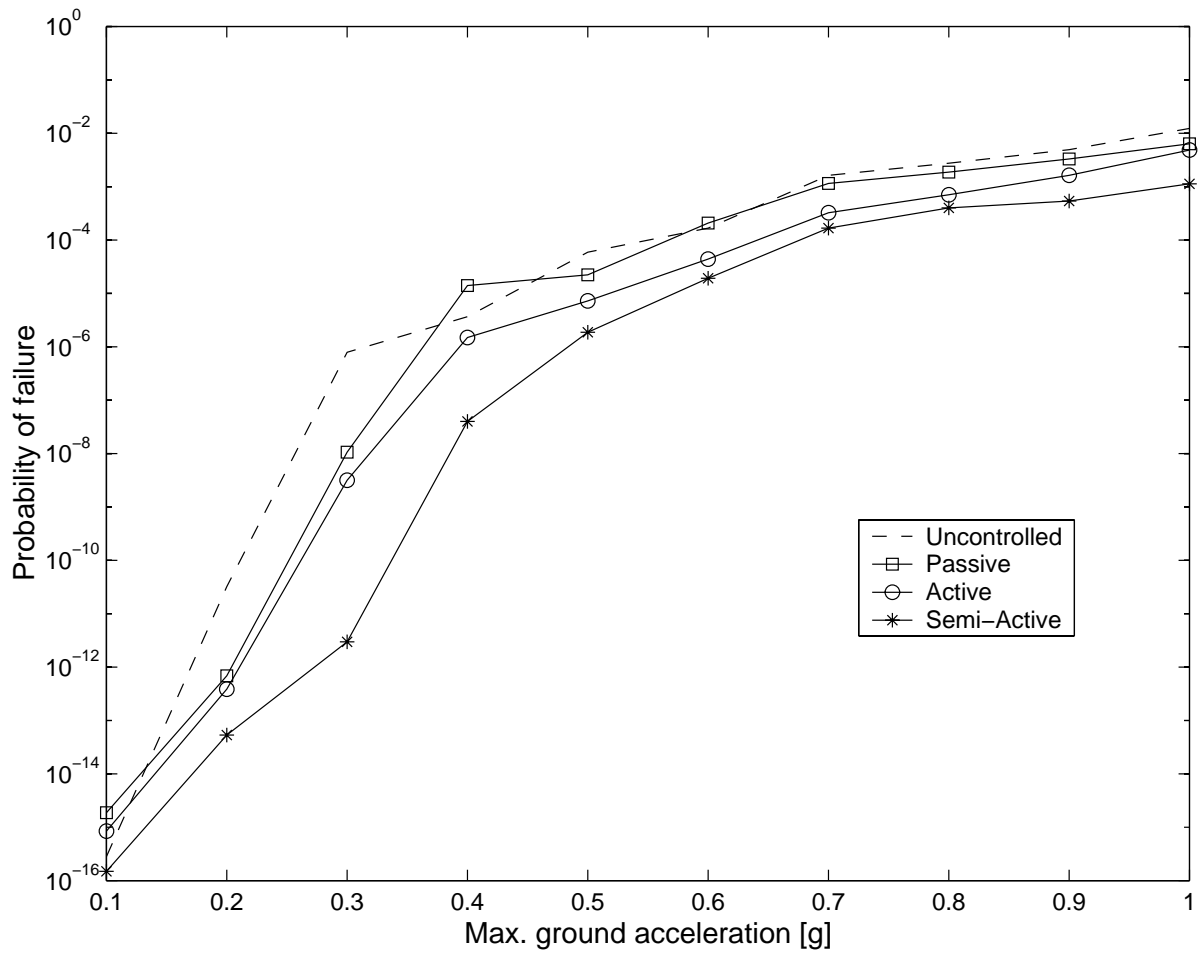


Figure 4.20 Fragility curves of the rail for different control methods.

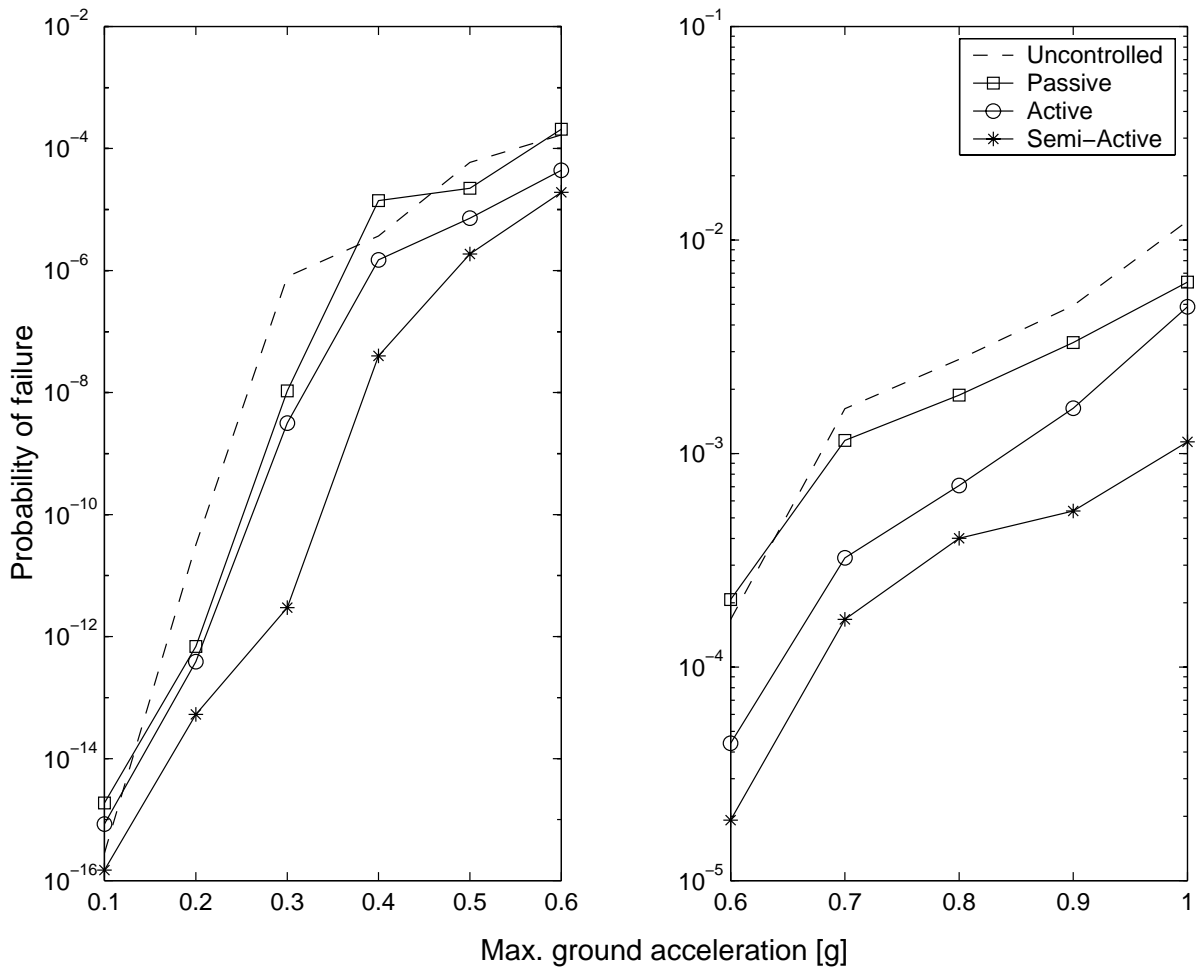


Figure 4.21 Fragility curves of the rail for different control methods.

Table 4.1
 Maximum stress in the rail for El Centro (0.348g) earthquake
 Mass ratio = 10%, Frequency ratio = 0.9

	Max. stress [ksi]	Reduction[%]
Uncontrolled	28.9520	--
Passive TMD	25.7339	11.12
Active TMD	23.6941	18.16
Passive MR Damper (0 V)	22.7673	21.36
Passive MR Damper (2.25 V)	23.9665	17.22
Semi-active MR Damper	21.8636	24.48

Table 4.2
 Maximum stress in the rail for Northridge (0.843g) earthquake
 Mass ratio = 10%, Frequency ratio = 0.9

	Max. stress [ksi]	Reduction[%]
Uncontrolled	55.1143	--
Passive TMD	46.5939	15.46
Active TMD	44.7498	18.81
Passive MR Damper (0 V)	45.9617	16.61
Passive MR Damper (2.25 V)	46.0900	16.37
Semi-active MR Damper	45.4408	17.55

Table 4.3
 Maximum stress in the rail for El Centro (0.348g) earthquake
 Mass ratio = 20%, Frequency ratio = 0.9

	Max. stress [ksi]	Reduction[%]
Uncontrolled	28.9520	--
Passive TMD	25.7028	11.22
Active TMD	24.5658	15.15
Passive MR Damper (0 V)	23.3556	19.33
Passive MR Damper (2.25 V)	22.2728	23.07
Semi-active MR Damper	21.5015	25.73

Table 4.4
 Maximum stress in the rail for Northridge (0.843g) earthquake
 Mass ratio = 20%, Frequency ratio = 0.9

	Max. stress [ksi]	Reduction[%]
Uncontrolled	55.1143	--
Passive TMD	44.9201	18.50
Active TMD	43.6230	20.85
Passive MR Damper (0 V)	43.9592	20.24
Passive MR Damper (2.25 V)	45.1662	18.05
Semi-active MR Damper	43.7567	20.61